

Photophysical Properties of Phenacylphenantridine Difluoroboranyls: Effect of Substituent and Double Benzannulation

Anna Maria Grabarz,[†] Beata Jędrzejewska,[‡] Anna Zakrzewska,[‡] Robert Zaleśny,[†] Adèle D. Laurent,[§] Denis Jacquemin,^{*,§} and Borys Ośmiałowski^{*,‡}

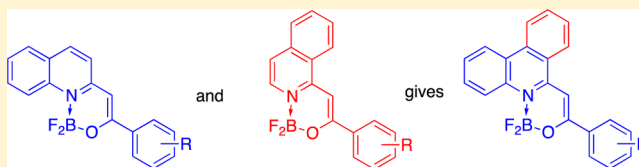
[†]Department of Physical and Quantum Chemistry, Faculty of Chemistry, Wrocław University of Science and Technology, Wyb. Wyspiańskiego 27, PL-50370 Wrocław, Poland

[‡]Faculty of Chemical Technology and Engineering, UTP University of Science and Technology, Seminaryjna 3, PL-85326 Bydgoszcz, Poland

[§]Laboratoire CEISAM, UMR CNRS 6230, Université de Nantes, 2 Rue de la Houssinière, BP92208, 44322 Cedex 3 Nantes, France

Supporting Information

ABSTRACT: In this study we present a new series of phenantridine-based substituted difluoroboranyls. The effects of substitution and double benzannulation on their photophysical properties were examined with experimental techniques and compared with the results obtained for previously reported quinoline and isoquinoline derivatives. The experimental characterizations are supported by state-of-the-art quantum-chemical calculations. In particular, the theoretical calculations were performed to gain insights into the complex nature of the relevant excited-states. These calculations reveal that both the nature of the substituent and its position on the phenyl ring significantly impact the magnitude of the electronic charge transferred upon excitation. Additionally, vibrationally resolved spectra were determined allowing for the analysis of the key vibrations playing a role in the band shapes.



INTRODUCTION

BODIPYs are strongly fluorescent molecules that have been exploited in many fields of science.^{1–6} In BODIPYs, a central BF₂ group is tethered between two pyrrole rings (Figure 1a),

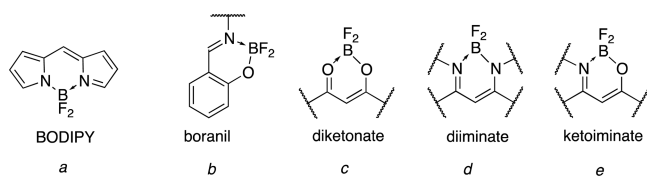


Figure 1. Structure of the cores of various classes of BF₂ carrying molecules.

ensuring a planar π -conjugated path between the two nitrogen atoms that are separated by three carbon atoms. As a formal positive charge is delocalized on this path, BODIPYs present many spectral features similar to classical merocyanine dyes,⁷ including sharp and intense absorption and emission bands each accompanied by a shoulder. The core of BODIPYs is obtained through a reaction in which the NH proton of one of the pyrrole rings is replaced by BF₂ moiety. A similar process allows obtaining boranil derivatives (Figure 1b).^{8,9} However, in that event the proton of an OH group is substituted in the last step of the synthetic route leading to a N–B–O type linkage. Yet another class of compounds with BF₂ moiety are diketonates (Figure 1c) that also constitute an increasingly popular family,^{10–18} whereas diiminates^{19–21} (with BF₂ bonded to two

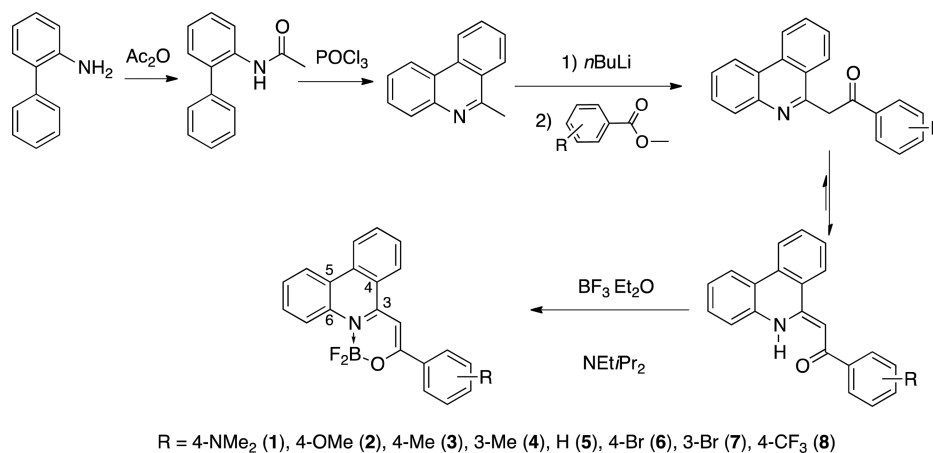
nitrogen atoms) (Figure 1d) as well as ketoiminates^{22–30} (Figure 1e) with unsymmetrically bonded BF₂ moiety have also been studied. Globally, the BF₂-carrying molecules are the most popular organic fluorophores to date and, as Zissel pointed out, they constitute an “El Dorado for fluorescence tools”.³¹ Some BODIPYs exhibit near-infrared (NIR) fluorescence in solution^{32–34} but also as a film on surfaces,³⁵ so that several have been used as red photon harvesters in solar cells.^{36–41} However, the fluorescence quantum yields remain rather small for the most red-shifted emitters. To lift this limitation, it is important to understand the key parameters controlling the emission properties so to allow the rational and systematic tuning of the spectroscopic features, further paving the way toward applications of these dyes in several fields, e.g., bioimaging^{4,42,43} and sensing.^{44–49}

It is known that the properties of dyes may be tuned by a numerous methods, including: (i) varying the heteroatoms involved in the excited-state, e.g., replacing nitrogen by oxygen atoms (diketonates versus ketoiminates versus diiminates); (ii) substituting molecular fragments with electroactive groups to benefit from Hammett’s correlation;^{50,51} and (iii) increasing the π -conjugation length, notably in compounds exhibiting photo-induced charge transfer (CT).^{52,53} In fact, we have recently demonstrated that the control of the conjugation path can be successfully applied to tune the optical properties of

Received: November 12, 2016

Published: January 9, 2017

Scheme 1. Synthesis of Substituted (Z)-6-(2-((Difluoroboryl)oxy)-2-phenylvinyl)phenanthridines



difluoroboranyls.⁵² Moreover, we have also started to explore the impact of benzannulation of the central pyridine ring in several BF₂-carrying molecules.^{23,24}

The fusion of benzo ring(s) with the central core of a conjugated molecule can greatly impact its properties, as demonstrated by several studies on various compounds, including polyacenes.^{54–58} In addition, benzannulation may change the energy of the transition state in proton transfer reaction,⁵⁹ tune the position of the proton (enol carrying OH group or enamine carrying NH group) in a series of tautomerizable CH-acids,^{50,51,60} as well as the photophysical properties of organic compounds. For instance both blue- and red-shifts of the absorption spectra have been observed depending on the position of the benzannulation.⁵⁶ These auxochromic effects can be important, e.g., the red-shift of the absorption band after benzannulation can be as large as 121 nm.^{61,62} Moreover, it is known that benzannulation may render the other fused rings less aromatic. This effect is dependent on the ring connectivity pattern and can be described by the Clar's⁶³ rule, which states that the properties of polycyclic aromatic molecules can be explained by the localization of the aromatic sextet. More precisely, this rule is to "assign the π -electrons that can participate in aromatic sextets to particular rings and to do so in such a way as to obtain the maximum number of π -electron sextets".⁶⁴ This empirical model is of invaluable help for explaining and predicting the structure and reactivity of benzenoid species.⁶⁵ For instance, according to Clar's rule the central ring in triphenylene is nonaromatic,^{66,67} and this has important consequences on the electron accepting properties of such ring. In short, π -electron conjugation (benzannulation) influences the properties of conjugated molecules both quantitatively and qualitatively.

Benzannulated BODIPYs and related dyes have been reported by Vicente,⁶⁸ Gresser,⁶¹ Kubo,^{62,69} and others.^{70–73} We underline that, in classical BODIPY dyes, the pyrrole ring cannot be doubly benzannulated due to the topology of the BODIPY core. To the best of our knowledge, the impact of double benzannulation with simultaneous variation of the substituent of the phenyl ring(s) on the photophysical properties of difluoroboranyls has not been systematically addressed to date. Nevertheless, we have recently shown that quinoline²³ derivatives differ significantly (especially in fluorescent quantum yields) from their isoquinoline counterparts.²⁴ Consequently, varying the position of the benzo ring attached to the heterocyclic one is a potentially interesting route for

obtaining different photophysical properties. Moreover, following Clar's rule one can use the benzannulation of the heterocyclic ring to lower its aromatic character and hence modify the emission spectrum of these fluorophores.

In the present study we perform a joint experimental and theoretical analysis of eight novel dyes (1–8 in Scheme 1).

We aim to (i) analyze whether the substituent effect (R in Scheme 1) in phenanthridine-based difluoroboranyls is similar to the one determined in the corresponding quinoline (Figure 2a)

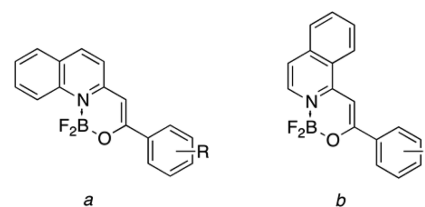


Figure 2. Structures of quinoline (a) and isoquinoline (b) derivatives.

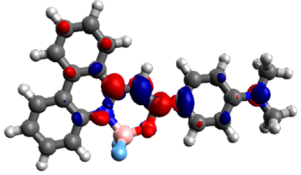
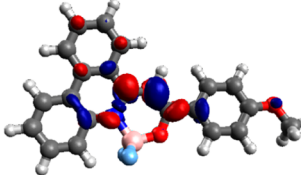

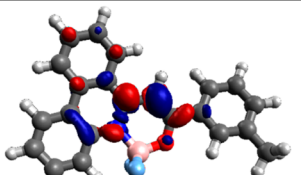
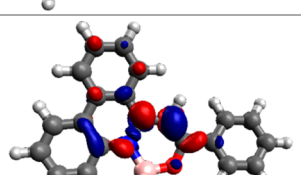
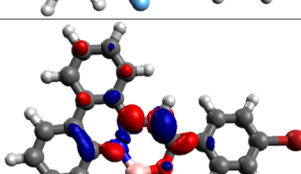
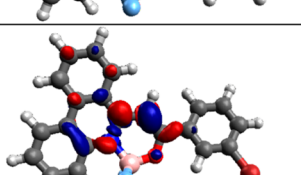
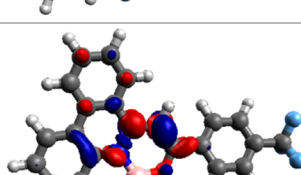
and isoquinoline (Figure 2b) derivatives; (ii) assess the effect of double benzannulation on the photophysical properties of variable substituted difluoroboranyls; and (iii) compare the properties of these dyes to those of quinoline and isoquinoline series. This study is therefore a further step in our efforts in this field^{23,24} and is dedicated to phenanthridine-based difluoroboranyls.

RESULTS AND DISCUSSION

The title compounds were synthesized using a described method^{23,24} taking 6-phenacylphenanthridines as substrates in reaction with BF₃ etherate. Scheme 1 summarizes the synthetic path described in detail previously; 6-methylphenanthridine was obtained according to procedure by Morgan⁷⁴ while this compound was reacted with commercially available substituted benzoic acid esters giving 6-phenacylphenanthridines characterized as before.⁶⁰

We start our discussion by presenting the theoretical results obtained for the lowest-energy electronic transition in the examined series, as these results provide information useful for further discussion. To understand the nature of the lowest-energy excited state we determined the density difference plots for each compound (see Table 1). As can be seen, the excited state is mainly localized on the BF₂-carrying ring and the adjacent heterocyclic ring. Notably, for molecules containing a

Table 1. Density Difference Plots and CT Parameters for the Investigated Compounds^{a,b}

Structure	Density difference plot	d_{CT} [Å]	q_{CT} [e]	$\Delta\mu_{CT}$ [D]
1		2.82	0.58	4.92
2		1.45	0.49	-0.04
3		0.94	0.46	-1.00
4		0.77	0.46	-1.21
5		0.69	0.46	-1.27
6		0.72	0.46	-1.44
7		0.54	0.46	-1.21
8		0.51	0.46	-0.64

^aWe report the CT distance (Å), charge (e), and the change of dipole moment (D) between the ground and excited states. ^bThe blue (red) zones indicate density decrease (increase) upon transition from the ground to the excited state.

strong electron-donating group (1 and also 2 to a lesser extent) one can observe a significant loss of the density on the

corresponding C_6H_4-R fragments upon transition. The strong CT in 1 is also reflected in the increased value of the transferred charge, q_{CT} , for 1 (0.56 e) compared to the other dyes, for which q_{CT} attains ca. 0.46 e , regardless of the substituent. In contrast, both the nature of the substituent and its position on the phenyl ring significantly impact the charge transfer distance, d_{CT} , which varies from 0.5 to 2.8 Å in the considered series. As expected, using the parent compound 5 as reference, smaller d_{CT} are obtained with the electron-withdrawing groups (CF_3 and Br), whereas larger distances are reached with strong electron-donating groups in position 4 of the phenyl ring that maximizes CT. The change of dipole moment $\Delta\mu_{CT}$ is also dependent on the substituent attached to phenyl ring: 1 exhibits a moderate increase of its dipole after photon absorption (ca. 5 D), whereas, for the rest of the examined compounds, the $\Delta\mu_{CT}$ values are small and slightly negative indicating that there is clearly no clear-cut CT nature in compounds 2–8. Consistently with this analysis, theory predicts negligible bathochromic shifts compared to 5 for all dyes except for 1 for which a substantial red-shift is predicted, 60 nm. This value accurately matches its experimental counterpart of 72 nm (see below).

In Figures 3 and 4 we report the electronic absorption and emission spectra measured in chloroform for compounds 1–8,

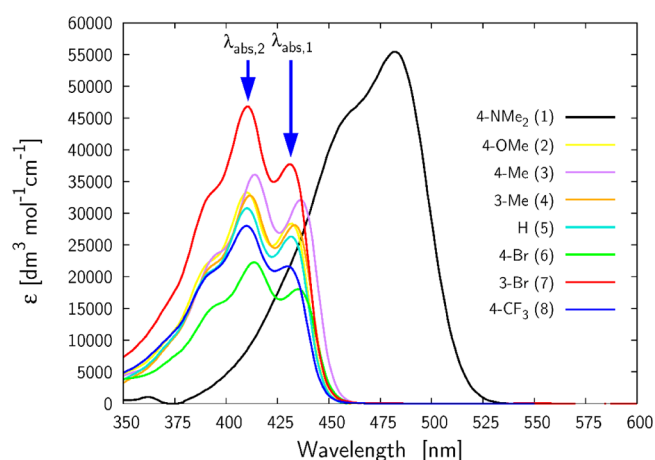


Figure 3. Measured electronic absorption spectra of compounds 1–8 in chloroform at r.t.

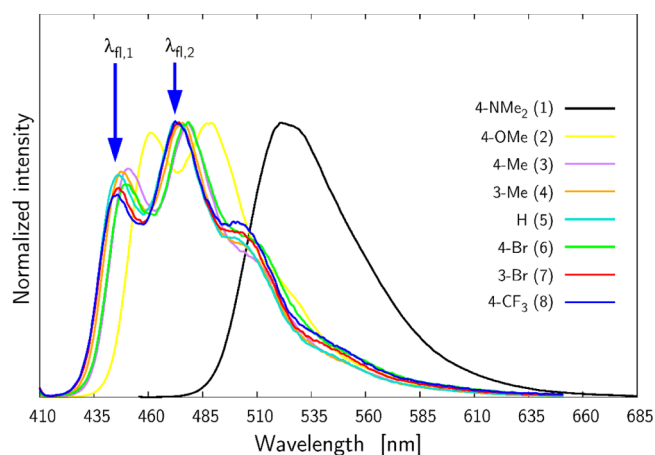


Figure 4. Electronic emission spectra for compounds 1–8 in chloroform.

Table 2. Main Photophysical Parameters^a for Compounds under Study in CHCl₃

comp	$\lambda_{\text{abs},1}$	ϵ	$\lambda_{\text{fl},1}$	ϕ_{fl}	τ_1	τ_2	τ_{av}	χ^2	k_r	k_{nr}
	$\lambda_{\text{abs},2}$		$\lambda_{\text{fl},2}$		α_1	α_2				
1	483	55500	521	0.811	0.198	2.652	2.595	1.65	3.12	0.07
					2.31	97.69				
2	444		461		0.631	1.769				
	420	33300	484	0.678	16.26	83.74	1.584	1.36	4.28	0.20
3	437		450		0.335	0.779				
	414	36100	478	0.275	16.45	83.55	0.706	1.17	3.90	1.03
4	434		447		0.059	0.553				
	412	32800	478	0.188	25.22	74.78	0.428	1.78	4.39	1.90
5	432		447		0.031	0.408				
	410	30800	473	0.131	11.80	88.10	0.363	1.92	3.61	2.39
6	435		449		0.365	0.632				
	414	22300	478	0.152	74.33	25.67	0.436	1.48	3.49	1.95
7	432		446		0.089	0.358				
	411	46800	473	0.106	15.89	84.11	0.315	1.84	3.36	2.84
8	430		446		0.019	0.294				
	410	28000	472	0.089	17.05	82.95	0.247	1.69	3.60	3.69

^aAbsorption maxima (λ_{abs} ; nm), maximum extinction coefficient (ϵ ; $\text{M}^{-1} \text{cm}^{-1}$), fluorescence maxima (λ_{fl} ; nm), fluorescence quantum yield (ϕ_{fl}), fluorescence lifetime (τ ; ns), its amplitude (α) and correlation coefficient (χ^2), radiative (k_r ; 10^8 s^{-1}) and nonradiative (k_{nr} ; 10^9 s^{-1}) rate constants for compounds under study.

whereas Table 2 collects the experimental spectral parameters for both absorption and emission in the same solvent. Chloroform was chosen as, on the one hand, BF₂-carrying molecules are stable in this medium and, on the other hand, similar compounds do not aggregate at the selected concentrations.²³ As can be seen, all compounds exhibit intense absorption in the visible part of the electronic UV-vis spectrum. For 1 and 8 other solvents were also investigated (see below).

The influence of the substituent on the position of the main absorption band remains relatively limited in most cases. Indeed, for compounds 2–8 the substituent induces variations of the $\lambda_{\text{abs},1}$ and $\lambda_{\text{abs},2}$ limited to 7 nm only. The largest change is unsurprisingly obtained for the strongest donor group, namely the 4-NMe₂ derivative (1) that induces the appearance of a red-shifted CT excited state consistently with the above analysis. The molar absorption coefficient (ϵ) in the 1–8 series varies between 22 300 and 55 500 $\text{dm}^3 \text{mol}^{-1} \text{cm}^{-1}$ (Table 2), the lowest and highest values being found for 6 (4-Br) and 1 (4-NMe₂), respectively. These values are globally of the same order of magnitude as in their quinoline²³ and isoquinoline²⁴ counterparts. For 1 (4-NMe₂) the measured ϵ (55 500 $\text{M}^{-1} \text{cm}^{-1}$, see Table 2) is almost the same as in the corresponding quinoline (56 500 $\text{M}^{-1} \text{cm}^{-1}$) and significantly higher than in the 4-NMe₂ substituted isoquinoline (31 500 $\text{M}^{-1} \text{cm}^{-1}$). This clearly suggests that adding the benzo ring at the 5,6-position (Scheme 1) of the heterocyclic ring has a larger impact on the spectral properties than that at the 3,4-position, at least for the compounds displaying substantial CT. This statement also holds when the absorption maxima are considered. Indeed, a comparison between the isoquinoline, quinoline, and phenanthridine dyes studied here leads to the same conclusion, e.g., the difference between 4-NMe₂ substituted quinoline and phenanthridine, and, isoquinoline and phenanthridine are 260 and 755 cm^{-1} , respectively. In short, our studies show that benzannulation in 5,6-position induces larger effects than the corresponding substitution in the 3,4-position.

The comparison of 1–8 with the respective (iso)quinolines shows that the electronic absorption spectra of the two dye series share very similar topologies.^{23,24} The theoretical

calculations reveal that the main absorption band corresponds to the lowest-lying $\pi-\pi^*$ transition, which is characterized by large oscillator strength [varying from 0.87 (5) to 1.3 (1)], consistently with the large measured ϵ . As expected, these transitions can be ascribed to one-electron HOMO–LUMO excitation (in the case of 1 a non-negligible contribution from HOMO–1 to LUMO transition is additionally present). From Figure 5 one can see that the differences between experimental

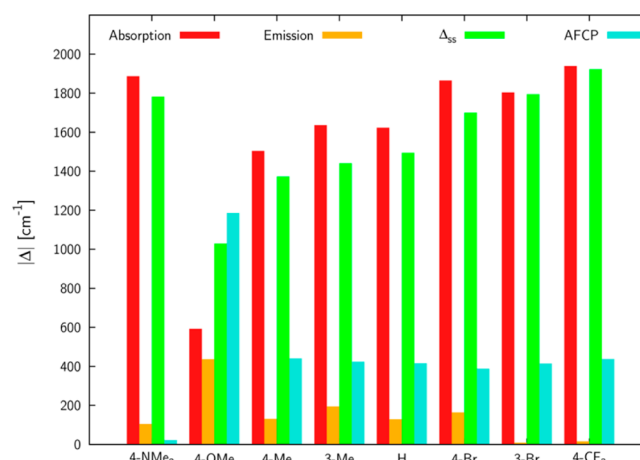


Figure 5. Unsigned differences between experimental and simulated spectral features (see text for more details).

and simulated absorption range from 590 cm^{-1} (2) to 1940 cm^{-1} (8). However, we underline that these theoretical absorption and emission maxima have been calculated within the vertical approximation. This means that the corresponding transition energies are computed with a frozen GS geometry and therefore the vibrational degrees of freedom and hence vibronic effects are neglected. That is why we also compare theoretical and experimental 0–0 energies in Table S1 of the SI.⁷⁵

The electronic emission spectra of compounds 1–8 depicted in Figure 4 exhibit similar trends as the one obtained for absorption. Indeed, the emission spectral shifts in the 2–8 series

are negligible (with **2** the maximal shift is 9 nm), whereas for **1** a large bathochromic shift of 74 nm is observed compared to the most intense peak in the vibronic progression ($\lambda_{fl,2}$) of the parent compound (**5**). This observation, together with the fact that the vibronic structure is washed out in **1** clearly confirms that this dye presents a CT nature, whereas the other compounds present rather localized π - π^* excited-states.

Further evidence that the structure of compound **1** allows for an efficient intramolecular CT comes from the solvatochromism of its optical properties. We have compared the absorption and emission of **1** recorded in methylcyclohexane (MCH), tetrahydrofuran (THF), and dimethyl sulfoxide (DMSO) with the corresponding results for **8** that bears a strong electron withdrawing group (see Figures S1–S5 in the SI). An increase of the solvent polarity induces red-shifts of the absorption and fluorescence bands position for both compounds. However, this effect is much more pronounced for **1** than for **8**. In fact, when the solvent is changed from MCH to DMSO, the absorption and fluorescence maxima of compound **1** are red-shifted by 12 and 108 nm, respectively, whereas the corresponding values are 2 and 5 nm for **8**. The considerable red-shift of the absorption and fluorescence bands position for compound **1** indicates that the difference between the excited- and ground-state charge distribution is larger and that the stabilization of the excited-state is large in polar solvents. Such behavior reflects the increase of solute–solvent interactions and is characteristic of CT compounds that present an increase in the dipole moment upon excitation, consistently with the theoretical values reported in Table 1.⁷⁶

The analysis of the fluorescence excitation spectra, recorded at various wavelengths and compared with the absorption spectra, showed that the fluorescence excitation spectra have slightly larger width than the absorption spectra which may suggest that there are small differences in spatial conformations and/or in solvent relaxation of the excited molecules.

The largest fluorescence quantum yield (ϕ_{fl}) is obtained for **1**, which is rather surprising considering the CT nature of this compound and the red-shifted nature of its emission. Nonetheless our theoretical calculation revealed that the structures of all examined compounds tend to be more planar in their excited state than in their ground state, i.e., the $\text{CH}=\text{C}(-\text{OBF}_2)$ -*Cipso-Cortho* dihedral angles between the CC double bond and the phenyl ring attains 3° in **1** and 2° in **5**, whereas the corresponding ground-state values are 13° (**1**) and 21° (**5**) which in turn can explain the unusually large ϕ_{fl} value: the geometry of **1** evolves less after photon absorption and the subsequent relaxation is more limited than in the other dyes. Finally, by looking at Figure 5 we notice a surprisingly good agreement between the simulated emission and experimental data (errors below 500 cm^{-1}), despite the limitations of the vertical approach (see the discussion above regarding photo-absorption process).

Following the trends of the experimental absorption and emission data, the Stokes shifts, Δ_{ss} are rather small in **2–8** ranging from 687 (**3**) up to 856 cm^{-1} (**2**), whereas a value twice larger, but still rather modest, is obtained for **1** (1510 cm^{-1}). As can be seen from Figure 5 the errors in the calculated Δ_{ss} follow the discrepancies noted for the absorption and therefore range from 1028 (**2**) to 1923 cm^{-1} (**8**).

Consistently with these trends, the 0–0 energy is only marginally dependent on the substituent but for **1** (see Table S1 in the SI). Interestingly, the computed 0–0 energies stay in excellent agreement with their experimental counterparts, with

an average overestimation as small as 460 cm^{-1} . As already stated above, 0–0 energies allow physically sound comparisons between theory and experimental data. We also highlight that a large linear determination coefficient ($R^2 > 0.90$; see Figure S4 in the SI) between experimental and simulated 0–0 energies has been obtained, confirming that the used level of theory is suitable.

The fluorescence quantum yields of **1–8** and the associated nonradiative rate constants are of the same order of magnitude as in isoquinolines. Plots comparing these values between the three series (phenanthridine, quinoline, and isoquinoline) are available in Figure S2 in the SI. The time-resolved fluorescence measurements revealed that there are two fluorescence lifetimes in the phenanthridine series (Figure S19). The fast decay lifetime (ps) of the compounds might be attributed to fluorescence from the nonrelaxed excited state, whereas the relaxed excited state is probably responsible for the nanosecond fluorescence lifetime.

The short fluorescence lifetime (τ_1) for **1–8** behaves irregularly with the substituent. This is in contrast with isoquinolines where τ_1 was found linearly dependent on the Hammett constant of the substituent. For τ_2 , the long fluorescence lifetime, our data suggest that the dependence pattern is intermediate between quinolines and isoquinolines (see Figure S1 in the SI) leading to the conclusion that benzannulation in 5,6 position controls the τ_2 . We note that the k_r amplitudes of phenanthridines follow the trends observed for quinolines and that the 4-NMe₂ substituted dye exhibits the smallest value in the series (contrasting with the isoquinoline series, for which the reverse was observed).

Besides CHCl₃, the fluorescence decay curves of compound **1** were also recorded in MCH, THF, and DMSO (see Figure S20). As the solvent polarity increases, we observed that the fast fluorescence lifetime is reduced and its contribution in the total emission decreases. This is accompanied by a rise in the relative importance of the slow decay component. Thus, we can speculate that the fast decay component for compound **1** originates from the nonrelaxed ICT state, whereas the slow decay component results from the relaxed ICT state.

By and large, phenanthridine derivatives resemble more quinolines than isoquinolines. This may be due to stronger benzannulation effect in the 5,6 position than in the 3,4 position. Alternatively these effects may be caused by interaction of the fluorine atoms with the CH aromatic proton (possible only for quinoline and phenanthridine derivatives) that could influence the electronic distribution within molecule. The CH/F through space coupling was detected in the ¹H NMR spectra as broadened doublet signal tending to doublet of triplets (proton in close proximity of fluorines). A similar weak CH...F interaction has been used in recognition of hydrocarbons⁷⁷ so, presumably, this kind of interaction may play a role in the present compounds.

As can be seen in Figures 3 and 4, the spectra of **2–8** exhibit fine structure, characterized by two distinct absorption (fluorescence) bands in the visible range, whereas the absorption and emission spectra for **1** are rather structureless. We therefore performed vibrationally resolved calculations, relying on formerly estimated inhomogeneous broadenings, see Computational Details Section. Our results are displayed in Figure 6 (see also Figures S6–S13 in the SI) and the simulated band topologies very nicely match the experimental data although for **1** the theoretical spectra is slightly too narrow compared to experiment. Of course, the simulated curves tend to be shifted with respect to their experimental counterparts,

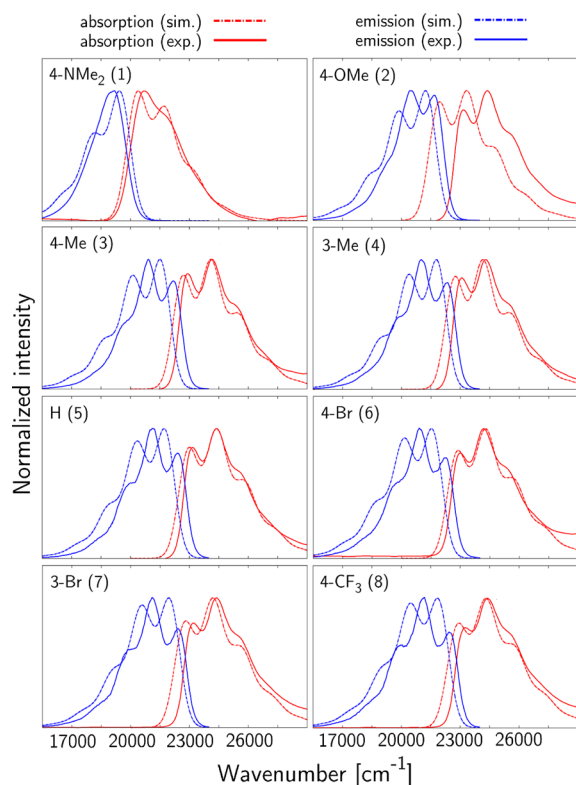


Figure 6. Comparison between experimental and simulated absorption and fluorescence spectra for 1–8.

following the already mentioned slight theoretical underestimation of the 0–0 energies. Additionally, we identified the key vibrational modes associated with the dominant components in the vibrational progression. As expected, the most intense normal modes contributing to absorption band correspond to combinations of the asymmetric wagging C–H vibrations and asymmetric C–C stretching of double bonds. The frequencies of the most important mode range from 1571 (1) up to 1630 cm^{-1} (7) depending on compound (See Table S2 in the SI for representation).

It is worth to note that the main difference between the compounds studied here and BODIPY dyes is in the ease of functionalization of the molecules described herein. The effects resulting from substitution and benzannulation are not easy to address in BODIPYs due to their five-membered ring that cannot be doubly benzannulated as the six-membered one. The main disadvantage of BODIPY dyes is the relatively small Stokes shifts that causes self-quenching. There are known BODIPY dyes^{78,79} that are characterized by relatively large Stokes shifts (higher than 100 nm⁷⁸) but their fluorescence quantum yield is low. The double benzannulation rigidifies the structure of molecule and creates opportunity to join spectral features between other series (Figure S2). Those are not yet met in BODIPY dyes.

CONCLUSIONS

We have synthesized and examined the optical properties of a series of novel phenanthridine-based difluoroboranyl fluorophores. The evolutions induced by substituent effects globally parallel the ones observed in the corresponding isoquinolines and/or quinolines. Consequently, for the compounds containing the strongest donor group, namely, dimethylamine, a significant bathochromic shift of both absorption and emission

spectra is observed, whereas, in the other cases, the auxochromic variations are trifling. It was observed in the previously described difluoroboranyl^{23,24} that NMe₂-carrying molecules differ significantly, and we show here that this is due to the CT character of these compounds. Depending on the selected properties phenanthridine dyes resemble their quinoline or isoquinoline counterparts (see details in the Results and Discussion Section). Notably, comparing NMe₂ derivatives only, the Stokes shift decreases following the isoquinoline, quinoline, and phenanthridine order. Nevertheless, the fluorescence quantum yield is the highest for the NMe₂ derivative here, a surprising result. One of the possible explanations is that the quinoid-like structure limits the excited-state flexibility, a suggestion substantiated by the small geometrical reorganization between the two electronic states evidenced by theoretical calculations. Of course, single and double benzannulation causes not only red-shifts of the absorption and emission maxima but also influences the rigidity of the molecule and hence the nonradiative decay rates. Clearly, rigidification accompanied by a shift of the emission toward longer wavelength preserving high fluorescence quantum yield may be a method of choice in tuning properties of fluorophores. This stiffening of the molecular core can also be seen in the strong vibronic structures that increase in the isoquinoline, quionoline, and phenanthridine order (Figure S3). Overall, the described photophysical properties are well supported by the *ab initio* computations that not only reproduced all main trends almost quantitatively, but also allowed to show that CT is only significant in 1.

EXPERIMENTAL SECTION

1,1-Difluoro-3-(4-dimethylaminophenyl)-1H-[1,3,2]-oxazaborinino[3,4-f]phenanthridin-13-ium-1-uide (1, R = 4-NMe₂). Yield 0.26 g (45.2%). mp 239.3–242.0 °C (EtOH), red powder (lit.²⁹ 237.2–238.4 °C). ¹H NMR (400 MHz, from TMS, DMSO-*d*₆): δ (ppm) 9.04 (d, 1H, ³J_{H,H} = 8.16 Hz), 8.84 (d, 1H, ³J_{H,H} = 7.96 Hz), 8.75 (d, 1H, ³J_{H,H} = 8.36 Hz), 8.49 (d, 1H, ³J_{H,H} = 8.36 Hz), 8.16 (d, 2H, ³J_{H,H} = 9.20 Hz), 8.08 (t, 1H), 7.87 (t, 1H), 7.76 (t, 1H), 7.65 (t, 1H), 7.52 (s, 1H), 6.84 (d, 2H, ³J_{H,H} = 9.20 Hz), 3.09 (s, 6H). ¹¹B (128 MHz, from BF₃·Et₂O, DMSO-*d*₆): δ (ppm) 2.256 (t). ¹³C (100 MHz, from TMS, DMSO-*d*₆): δ (ppm): 167.3, 155.0, 153.5, 135.7, 134.8, 133.0, 130.3, 129.8, 129.6, 128.7, 126.5, 123.8, 123.4, 123.1, 123.0, 122.7, 119.5, 111.8, 87.4, ca. 40 (overlapped by solvent). ¹⁵N (40 MHz, from MeNO₂, DMSO-*d*₆): δ (ppm): –198.0. ¹⁹F (376 MHz, from CFCl₃, DMSO-*d*₆): δ (ppm) –125.8. Anal. Calc. for C₂₂H₁₉BF₂N₂O: C 71.16, H 4.93, N 7.22. Found: C 70.95, H 5.01, N 7.01.

1,1-Difluoro-3-(4-methoxyphenyl)-1H-[1,3,2]oxazaborinino[3,4-f]phenanthridin-13-ium-1-uide (2, R = 4-OMe). Yield 0.39 g (56.7%). mp 253.5–254.2 °C (EtOH), light orange powder (lit.²⁹ 252.5–253.5 °C). ¹H NMR (400 MHz, from TMS, DMSO-*d*₆): δ (ppm) 9.11 (d, 1H, ³J_{H,H} = 8.48 Hz), 8.90 (d, 1H, ³J_{H,H} = 8.36 Hz), 8.82 (d, 1H, ³J_{H,H} = 8.24 Hz), 8.57 (d, 1H, ³J_{H,H} = 8.64 Hz), 8.29 (d, 2H, ³J_{H,H} = 8.82 Hz), 8.13 (t, 1H), 7.91 (t, 1H), 7.81 (t, 1H), 7.70 (t, 1H), 7.66 (s, 1H), 7.14 (d, 2H, ³J_{H,H} = 8.82 Hz), 3.90 (s, 3H). ¹¹B (128 MHz, from BF₃·Et₂O, DMSO-*d*₆): δ (ppm) 2.314 (t). ¹³C (100 MHz, from TMS, DMSO-*d*₆): δ (ppm): 166.0, 163.2, 155.4, 135.3, 135.2, 133.2, 130.5, 129.8, 129.7, 128.9, 127.2, 125.8, 123.9, 123.6, 123.4, 123.1, 122.8, 114.8, 89.1, 56.1. ¹⁵N (40 MHz, from MeNO₂, DMSO-*d*₆): δ (ppm): –201.2. ¹⁹F (376 MHz, from CFCl₃, DMSO-*d*₆): δ (ppm) –125.1. Anal. Calc. for C₂₂H₁₆BF₂N₂O₂: C 70.43, H 4.30, N 3.73. Found: C 70.15, H 4.54, N 3.90.

1,1-Difluoro-3-(p-tolyl)-1H-[1,3,2]oxazaborinino[3,4-f]phenanthridin-13-ium-1-uide (3, R = 4-Me). Yield 0.42 g (51.4%). mp 259.8–261.9 °C (EtOH), yellow powder. ¹H NMR (400 MHz, from TMS, DMSO-*d*₆): δ (ppm) 9.10 (d, 1H, ³J_{H,H} = 8.36 Hz), 8.90 (d, 1H, ³J_{H,H} = 8.24 Hz), 8.82 (d, 1H, ³J_{H,H} = 8.00 Hz), 8.59 (d, 1H, ³J_{H,H} = 8.32 Hz), 8.19 (d, 2H, ³J_{H,H} = 8.02 Hz), 8.13 (t, 1H), 7.91 (t, 1H), 7.84 (t, 1H), 7.73 (t, 1H), 7.70 (s, 1H), 7.40 (d, 2H, ³J_{H,H} = 8.02 Hz), 2.43

(s, 3H). ^{11}B (128 MHz, from $\text{BF}_3\cdot\text{Et}_2\text{O}$, $\text{DMSO}-d_6$): δ (ppm) 2.343 (t). ^{13}C (100 MHz, from TMS, $\text{DMSO}-d_6$) δ (ppm): 166.0, 155.5, 143.1, 135.3, 133.3, 130.8, 130.5, 130.0, 129.7, 129.0, 127.7, 127.4, 123.9, 123.7, 123.5, 123.3, 123.2, 122.7, 89.9, 21.6. ^{15}N (40 MHz, from MeNO_2 , $\text{DMSO}-d_6$) δ (ppm): -198.0 . ^{19}F (376 MHz, from CFCl_3 , $\text{DMSO}-d_6$) δ (ppm) -124.9 . Anal. Calc. for $\text{C}_{22}\text{H}_{16}\text{BF}_2\text{NO}$: C 73.57, H 4.49, N 3.90. Found: C 73.70, H 4.56, N 3.79.

1,1-Difluoro-3-(*m*-tolyl)-1H-[1,3,2]oxazaborinino[3,4-*f*]phenanthridin-13-ium-1-uide (4, R = 3-Me). Yield 0.32 g (49.9%). mp 212.7–215.2 °C (EtOH), yellow powder. ^1H NMR (400 MHz, from TMS, $\text{DMSO}-d_6$): δ (ppm) 9.13 (d, 1H, $^3J_{\text{H,H}} = 8.20$ Hz), 8.92 (d, 1H, $^3J_{\text{H,H}} = 8.00$ Hz), 8.85 (d, 1H, $^3J_{\text{H,H}} = 8.32$ Hz), 8.64 (d, 1H, $^3J_{\text{H,H}} = 8.56$ Hz), 8.10–8.20 (m, 3H), 7.94 (t, 1H), 7.87 (t, 1H), 7.76 (t, 1H), 7.75 (s, 1H), 7.45–7.55 (m, 2H), 2.49 (s, 3H). ^{11}B (128 MHz, from $\text{BF}_3\cdot\text{Et}_2\text{O}$, $\text{DMSO}-d_6$): δ (ppm) 2.355 (t). ^{13}C (100 MHz, from TMS, $\text{DMSO}-d_6$) δ (ppm): 165.9, 155.4, 138.8, 135.3, 135.2, 133.5, 133.4, 133.3, 130.6, 129.7, 129.2, 129.0, 128.0, 127.5, 124.9, 123.9, 123.8, 123.5, 123.3, 122.7, 90.4, 21.4. ^{15}N (40 MHz, from MeNO_2 , $\text{DMSO}-d_6$) δ (ppm): -198.4 . ^{19}F (376 MHz, from CFCl_3 , $\text{DMSO}-d_6$) δ (ppm) -124.8 . Anal. Calc. for $\text{C}_{22}\text{H}_{16}\text{BF}_2\text{NO}$: C 73.57, H 4.49, N 3.90. Found: C 73.44, H 4.53, N 3.71.

1,1-Difluoro-3-phenyl-1H-[1,3,2]oxazaborinino[3,4-*f*]phenanthridin-13-ium-1-uide (5, R = H). Yield 0.37 g (52.7%). mp 218.2–220.9 °C (lit.²⁹ 201.9–206.3 °C) (EtOH), yellow powder. ^1H NMR (400 MHz, from TMS, $\text{DMSO}-d_6$): δ (ppm) 9.18 (d, 1H, $^3J_{\text{H,H}} = 8.20$ Hz), 8.97 (d, 1H, $^3J_{\text{H,H}} = 8.00$ Hz), 8.89 (d, 1H, $^3J_{\text{H,H}} = 7.04$ Hz), 8.66 (d, 1H, $^3J_{\text{H,H}} = 8.58$ Hz), 8.36 (m, 2H), 8.19 (t, 1H), 7.97 (t, 1H), 7.88 (t, 1H), 7.81 (s, 1H), 7.78 (t, 1H), 7.62–7.73 (m, 3H). ^{11}B (128 MHz, from $\text{BF}_3\cdot\text{Et}_2\text{O}$, $\text{DMSO}-d_6$): δ (ppm) 2.367 (t). ^{13}C (100 MHz, from TMS, $\text{DMSO}-d_6$) δ (ppm): 165.7, 155.5, 135.4, 135.2, 133.5, 133.4, 132.7, 130.6, 129.8, 129.4, 129.1, 127.7, 127.6, 124.0, 123.9, 123.5, 123.3, 122.7, 90.5. ^{15}N (40 MHz, from MeNO_2 , $\text{DMSO}-d_6$) δ (ppm): -198.3 . ^{19}F (376 MHz, from CFCl_3 , $\text{DMSO}-d_6$) δ (ppm) -124.8 . Anal. Calc. for $\text{C}_{21}\text{H}_{14}\text{BF}_2\text{NO}$: C 73.08, H 4.09, N 4.06. Found: C 72.99, H 4.18, N 3.94.

3-(4-Bromophenyl)-1,1-difluoro-1H-[1,3,2]oxazaborinino[3,4-*f*]phenanthridin-13-ium-1-uide (6, R = 4-Br). Yield 0.42 g (46.2%). mp 265.8–267.8 °C (EtOH), yellow powder. ^1H NMR (400 MHz, from TMS, $\text{DMSO}-d_6$): δ (ppm) 9.16 (d, 1H, $^3J_{\text{H,H}} = 8.24$ Hz), 8.95 (d, 1H, $^3J_{\text{H,H}} = 8.04$ Hz), 8.87 (d, 1H, $^3J_{\text{H,H}} = 7.04$ Hz), 8.62 (d, 1H, $^3J_{\text{H,H}} = 8.80$ Hz), 8.26 (d, 2H, $^3J_{\text{H,H}} = 8.72$ Hz), 8.18 (t, 1H), 7.94 (t, 1H), 7.85 (t, 1H), 7.82 (d, 2H, $^3J_{\text{H,H}} = \text{ca. } 8.56$ Hz, overlapped with singlet), 7.81 (s, 1H), 7.75 (t, 1H). ^{11}B (128 MHz, from $\text{BF}_3\cdot\text{Et}_2\text{O}$, $\text{DMSO}-d_6$): δ (ppm) 2.335 (t). ^{13}C (100 MHz, from TMS, $\text{DMSO}-d_6$) δ (ppm): 164.3, 155.4, 135.5, 135.2, 133.5, 132.8, 132.4, 130.7, 129.8, 129.6, 129.1, 127.7, 126.5, 124.0, 123.9, 123.5, 123.3, 122.7, 90.9. ^{15}N (40 MHz, from MeNO_2 , $\text{DMSO}-d_6$) δ (ppm): -197.0 . ^{19}F (376 MHz, from CFCl_3 , $\text{DMSO}-d_6$) δ (ppm) -124.8 . Anal. Calc. for $\text{C}_{21}\text{H}_{13}\text{BrBF}_2\text{NO}$: C 59.48, H 3.09, N 3.30. Found: C 59.35, H 3.21, N 3.19.

3-(3-Bromophenyl)-1,1-difluoro-1H-[1,3,2]oxazaborinino[3,4-*f*]phenanthridin-13-ium-1-uide (7, R = 3-Br). Yield 0.44 g (50.3%). mp 263.2–265.4 °C (EtOH), yellow powder. ^1H NMR (400 MHz, from TMS, $\text{DMSO}-d_6$): δ (ppm) 9.25 (d, 1H, $^3J_{\text{H,H}} = 8.32$ Hz), 9.01 (d, 1H, $^3J_{\text{H,H}} = 8.16$ Hz), 8.92 (d, 1H, $^3J_{\text{H,H}} = 7.08$ Hz), 8.68 (d, 1H, $^3J_{\text{H,H}} = 8.64$ Hz), 8.58 (m, 1H), 8.34 (d, 1H, $^3J_{\text{H,H}} = 7.92$ Hz), 8.23 (t, 1H), 7.99 (t, 1H), 7.88–7.94 (m, 3H), 7.82 (t, 1H), 7.62 (t, 1H). ^{11}B (128 MHz, from $\text{BF}_3\cdot\text{Et}_2\text{O}$, $\text{DMSO}-d_6$): δ (ppm) 2.313 (t). ^{13}C (100 MHz, from TMS, $\text{DMSO}-d_6$) δ (ppm): 163.5, 155.4, 135.9, 135.6, 135.2, 135.1, 133.5, 131.5, 130.7, 130.0, 129.8, 129.3, 127.8, 126.5, 124.1, 124.0, 123.5, 123.4, 122.8, 122.7, 91.4. ^{15}N (40 MHz, from MeNO_2 , $\text{DMSO}-d_6$) δ (ppm): -194.6 . ^{19}F (376 MHz, from CFCl_3 , $\text{DMSO}-d_6$) δ (ppm) -124.76 . Anal. Calc. for $\text{C}_{21}\text{H}_{13}\text{BrBF}_2\text{NO}$: C 59.48, H 3.09, N 3.30. Found: C 59.38, H 3.27, N 3.21.

1,1-Difluoro-3-(4-(trifluoromethyl)phenyl)-1H-[1,3,2]oxazaborinino[3,4-*f*]phenanthridin-13-ium-1-uide (8, R = 4-CF₃). Yield 0.51 g (59.7%). mp 266.1–268.7 °C (EtOH), yellow powder. ^1H NMR (400 MHz, from TMS, $\text{DMSO}-d_6$): δ (ppm) 9.23 (d, 1H, $^3J_{\text{H,H}} = 8.22$ Hz), 9.01 (d, 1H, $^3J_{\text{H,H}} = 8.08$ Hz), 8.94 (d, 1H, $^3J_{\text{H,H}} = 7.08$ Hz), 8.70 (d, 1H, $^3J_{\text{H,H}} = 8.56$ Hz), 8.56 (d, 2H, $^3J_{\text{H,H}} = 8.20$ Hz),

8.23 (t, 1H), 8.01 (d, 2H, overlapped with triplet), ca. 8.02 (t, 1H), 7.95 (s, 1H), 7.92 (t, 1H), 7.84 (t, 1H). ^{11}B (128 MHz, from $\text{BF}_3\cdot\text{Et}_2\text{O}$, $\text{DMSO}-d_6$): δ (ppm) 2.376 (t). ^{13}C (100 MHz, from TMS, $\text{DMSO}-d_6$) δ (ppm): 163.4, 155.4, 137.5, 135.6, 135.1, 133.6, 131.9 (q, $^2J_{\text{CF}} = 31.3$ Hz), 130.7, 129.8, 129.2, 128.4, 128.0, 126.2 (q, $^2J_{\text{CF}} = 3.5$ Hz), 124.4 (q, $^1J_{\text{CF}} = 273$ Hz), 124.2, 124.1, 123.5, 123.2, 122.7, 92.2. ^{15}N (40 MHz, from MeNO_2 , $\text{DMSO}-d_6$) δ (ppm): -194.5 . ^{19}F (376 MHz, from CFCl_3 , $\text{DMSO}-d_6$) δ (ppm) -124.6 , -61.3 . Anal. Calc. for $\text{C}_{22}\text{H}_{13}\text{BF}_5\text{NO}$: C 63.96, H 3.17, N 3.39. Found: C 63.88, H 3.29, N 3.22.

■ COMPUTATIONAL DETAILS

In the present work we followed a previously proposed computational protocol, allowing for accurate predictions of the optical signatures of difluoroboranyl derivatives.^{80,81} In this approach, the structural parameters are determined using density functional theory (DFT) and its time-dependent extension (TD-DFT) for the ground and excited-states (GS and ES), respectively whereas the total and transition energies are corrected for the effect of contributions from the double excitations using the SOS-CIS(D) approach. All DFT and TD-DFT calculations were performed using the Gaussian 09⁸² program package. The default thresholds were improved by using a tightened optimization threshold (10^{-5} au on average residual forces) and a stricter self-consistent field convergence criterion (10^{-10} a.u.). Additionally, in all DFT and TD-DFT calculations, we used the ultrafine pruned grid, which consists of the 99 radial shells and 590 angular points per shell. The SOS-MP2 and SOS-CIS(D) energies were calculated using the Q-Chem package⁸³ using the resolution of identity scheme. To include solvation effect we took advantage of the polarizable continuum model (PCM)⁸⁴ in all DFT and TD-DFT calculations. The geometry optimizations and frequency calculations were carried out using linear response (LR-PCM) scheme, whereas total and transition energies were treated with corrected linear response (cLR-PCM) approach.⁸⁵

In more details, the selected protocol follows a multistep approach. First, the GS and ES geometries have been optimized with DFT and TD-DFT, respectively, and the vibrational frequencies of both states have been subsequently determined, using the M06-2X *meta*-GGA hybrid exchange-correlation functional,⁸⁶ which is known to be well-suited for simulations of optical band shapes of BF_2 -carrying compounds.⁸¹ These calculations were performed with the 6-31G(d) atomic basis set. All optimized structures correspond to true minima of the potential energy surface. Second, the transition energies which require a much larger atomic basis set, 6-311+G(2d,p), were determined in gas-phase with TD-M06-2X and SOS-CIS(D) and in condensed phase with cLR-PCM-TD-M06-2X. The values reported in this study correspond to the SOS-CIS(D) values corrected for solvent effects using the difference between the cLR-PCM and gas TD-DFT values. Third, the vibrationally resolved spectra have been obtained using independent-mode displaced harmonic oscillator (IMDHO) approach implemented in ORCA program.⁸⁷ The dimensionless normal mode displacements were computed based on the excited-state gradient using custom computer routine. In order to allow direct comparisons between the computed vibrationally resolved absorption bands and the experimental spectra, the broadening has to be estimated. To do so, we computed the Franck-Condon spectrum for each compound in chloroform solution and convoluted the stick spectra (broadened by Lorentzian, where HWHM = 10 cm^{-1}) with Gaussian spectral profile, where standard deviation (σ) was in the 200–600 cm^{-1} range. For each value of σ , we then determined an overlap parameter quantifying the differences between experimental and simulated band shapes (eq 1):

$$\beta = \left[\frac{\int [I^{\text{exptl}}(v) - I_{\text{FC}}^{\text{simul}}(v)]^2 dv}{\int [I^{\text{exptl}}(v)]^2 dv} \right]^{1/2} \quad (1)$$

Note that $\beta = 0$ for identical spectral profiles. The experimental and simulated bands were shifted to match the 0–0 transitions. The dependence of β on the standard deviation is illustrated in the SI. It

turns out that the best match between the simulated and experimental spectra in chloroform is found for all compounds for σ values in the range 410–470 cm^{-1} . In the body of the text, we assume the same broadening to simulate the emission spectra. Various approaches for estimating the inhomogeneous broadening are discussed elsewhere.^{88,89}

Finally, the density difference plots shown in the present study were obtained at the PCM-TD-M06-2X/6-311+G(2d,p) level and are represented with a contour threshold of 0.002 au. The charge-transfer parameters, namely, the charge-transfer distance, d_{CT} , and the amount of transferred charge, q_{CT} , have been determined following a Le Bahers procedure.^{90,91} The combination of these two values provides the norm of the dipole moment change upon absorption.

■ ASSOCIATED CONTENT

■ Supporting Information

The Supporting Information is available free of charge on the ACS Publications website at DOI: 10.1021/acs.joc.6b02732.

Figures showing comparisons between series of BF₂-carrying derivatives, spectroscopic parameters, normal-mode analysis for the vibronic couplings, Cartesian coordinates of the DFT-optimized structures, NMR spectra, fluorescence decay charts, and spectra comparison (PDF)

■ AUTHOR INFORMATION

Corresponding Authors

*E-mail: Denis.Jacquemin@univ-nantes.fr

*E-mail: borys.osmialowski@utp.edu.pl

ORCID

Denis Jacquemin: 0000-0002-4217-0708

Borys Osmialowski: 0000-0001-9118-9264

Notes

The authors declare no competing financial interest.

■ ACKNOWLEDGMENTS

D.J. acknowledges the European Research Council (ERC) and the Région des Pays de la Loire for financial support in the framework of a Starting Grant (Marches -278845) and the LumoMat project, respectively. This research used resources of (i) the GENCI-CINES/IDRIS; (ii) CCIPL (Centre de Calcul Intensif des Pays de Loire); (iii) a local Troy cluster and (iv) HPC resources from ArronaxPlus (grant ANR-11-EQPX-0004 funded by the French National Agency for Research). R.Z. acknowledges Polish Ministry of Science and Higher Education for the statutory activity subsidy for the Faculty of Chemistry of Wrocław University of Technology (No. 0401/0147/15). Financial support from the National Science Centre (Grant No. 2013/09/B/ST5/03550) is gratefully acknowledged.

■ REFERENCES

- (1) Loudet, A.; Burgess, K. *Chem. Rev.* **2007**, *107*, 4891.
- (2) Boens, N.; Leen, V.; Dehaen, W. *Chem. Soc. Rev.* **2012**, *41*, 1130.
- (3) Kamkaew, A.; Lim, S. H.; Lee, H. B.; Kiew, L. V.; Chung, L. Y.; Burgess, K. *Chem. Soc. Rev.* **2013**, *42*, 77.
- (4) Ni, Y.; Wu, J. *Org. Biomol. Chem.* **2014**, *12*, 3774.
- (5) Kowada, T.; Maeda, H.; Kikuchi, K. *Chem. Soc. Rev.* **2015**, *44*, 4953.
- (6) Boens, N.; Verbelen, B.; Dehaen, W. *Eur. J. Org. Chem.* **2015**, *2015*, 6577.
- (7) Pascal, S.; Haeefe, A.; Monnereau, C.; Charaf-Eddin, A.; Jacquemin, D.; Le Guennic, B.; Andraud, C.; Maury, O. *J. Phys. Chem. A* **2014**, *118*, 4038.

- (8) Frath, D.; Azizi, S.; Ulrich, G.; Retailleau, P.; Ziessel, R. *Org. Lett.* **2011**, *13*, 3414.
- (9) Frath, D.; Azizi, S.; Ulrich, G.; Ziessel, R. *Org. Lett.* **2012**, *14*, 4774.
- (10) Ono, K.; Yamaguchi, H.; Taga, K.; Saito, K.; Nishida, J.-i.; Yamashita, Y. *Org. Lett.* **2009**, *11*, 149.
- (11) Ono, K.; Hashizume, J.; Yamaguchi, H.; Tomura, M.; Nishida, J.-i.; Yamashita, Y. *Org. Lett.* **2009**, *11*, 4326.
- (12) Fedorenko, E. V.; Mirochnik, A. G.; Beloliptsev, A. Y.; Isakov, V. *Dyes Pigm.* **2014**, *109*, 181.
- (13) Xu, S.; Evans, R. E.; Liu, T.; Zhang, G.; Demas, J. N.; Trindle, C. O.; Fraser, C. L. *Inorg. Chem.* **2013**, *52*, 3597.
- (14) Tikhonov, S. A.; Vovna, V. I.; Gelfand, N. A.; Osmushko, I. S.; Fedorenko, E. V.; Mirochnik, A. G. *J. Phys. Chem. A* **2016**, *120*, 7361.
- (15) Morris, W. A.; Kolpaczynska, M.; Fraser, C. L. *J. Phys. Chem. C* **2016**, *120*, 22539.
- (16) Butler, T.; Morris, W. A.; Samonina-Kosicka, J.; Fraser, C. L. *ACS Appl. Mater. Interfaces* **2016**, *8*, 1242.
- (17) Morris, W. A.; Butler, T.; Kolpaczynska, M.; Fraser, C. L. *Mater. Chem. Front.* **2017**, *1*, 158–166.
- (18) Samonina-Kosicka, J.; DeRosa, C. A.; Morris, W. A.; Fan, Z.; Fraser, C. L. *Macromolecules* **2014**, *47*, 3736.
- (19) Gao, N.; Cheng, C.; Yu, C.; Hao, E.; Wang, S.; Wang, J.; Wei, Y.; Mu, X.; Jiao, L. *Dalton Trans.* **2014**, *43*, 7121.
- (20) Yoshii, R.; Hirose, A.; Tanaka, K.; Chujo, Y. *J. Am. Chem. Soc.* **2014**, *136*, 18131.
- (21) Wang, X.; Wu, Y.; Liu, Q.; Li, Z.; Yan, H.; Ji, C.; Duan, J.; Liu, Z. *Chem. Commun.* **2015**, *51*, 784.
- (22) Kubota, Y.; Kasatani, K.; Takai, H.; Funabiki, K.; Matsui, M. *Dalton Trans.* **2015**, *44*, 3326.
- (23) Zakrzewska, A.; Zalesny, R.; Kolehmainen, E.; Osmialowski, B.; Jędrzejewska, B.; Ågren, H.; Pietrzak, M. *Dyes Pigm.* **2013**, *99*, 957.
- (24) Osmialowski, B.; Zakrzewska, A.; Jędrzejewska, B.; Grabarz, A.; Zalesny, R.; Bartkowiak, W.; Kolehmainen, E. *J. Org. Chem.* **2015**, *80*, 2072.
- (25) Yao, Q.-C.; Wu, D.-E.; Ma, R.-Z.; Xia, M. *J. Organomet. Chem.* **2013**, *743*, 1.
- (26) Graser, M.; Kopacka, H.; Wurst, K.; Ruetz, M.; Kreutz, C. R.; Müller, T.; Hirtenlehner, C.; Monkowius, U.; Knör, G.; Bildstein, B. *Inorg. Chim. Acta* **2013**, *405*, 116.
- (27) Zhou, Y.; Xiao, Y.; Chi, S.; Qian, X. *Org. Lett.* **2008**, *10*, 633.
- (28) Feng, J.; Liang, B.; Wang, D.; Xue, L.; Li, X. *Org. Lett.* **2008**, *10*, 4437.
- (29) Wu, D.-E.; Lu, X.-L.; Xia, M. *New J. Chem.* **2015**, *39*, 6465.
- (30) Kubota, Y.; Hara, H.; Tanaka, S.; Funabiki, K.; Matsui, M. *Org. Lett.* **2011**, *13*, 6544.
- (31) Ziessel, R.; Ulrich, G.; Harriman, A. *New J. Chem.* **2007**, *31*, 496.
- (32) Donyagina, V. F.; Shimizu, S.; Kobayashi, N.; Lukyanets, E. A. *Tetrahedron Lett.* **2008**, *49*, 6152.
- (33) Goeb, S.; Ziessel, R. *Org. Lett.* **2007**, *9*, 737.
- (34) Xue, X.; Fang, H.; Chen, H.; Zhang, C.; Zhu, C.; Bai, Y.; He, W.; Guo, Z. *Dyes Pigm.* **2016**, *130*, 116.
- (35) Topka, M. R.; Dinolfo, P. H. *ACS Appl. Mater. Interfaces* **2015**, *7*, 8053.
- (36) Liao, J.; Zhao, H.; Xu, Y.; Cai, Z.; Peng, Z.; Zhang, W.; Zhou, W.; Li, B.; Zong, Q.; Yang, X. *Dyes Pigm.* **2016**, *128*, 131.
- (37) Kaneza, N.; Zhang, J.; Liu, H.; Archana, P. S.; Shan, Z.; Vasiliu, M.; Polansky, S. H.; Dixon, D. A.; Adams, R. E.; Schmehl, R. H.; Gupta, A.; Pan, S. *J. Phys. Chem. C* **2016**, *120*, 9068.
- (38) Kraner, S.; Widmer, J.; Benduhn, J.; Hieckmann, E.; Jägerle-Hoheisel, T.; Ullbrich, S.; Schütze, D.; Sebastian Radke, K.; Cuniberti, G.; Ortmann, F.; Lorenz-Rothe, M.; Meerheim, R.; Spoltore, D.; Vandewal, K.; Koerner, C.; Leo, K. *Phys. Status Solidi A* **2015**, *212*, 2747.
- (39) Mao, M.; Zhang, X.; Cao, L.; Tong, Y.; Wu, G. *Dyes Pigm.* **2015**, *117*, 28.
- (40) Cakmak, Y.; Kolemen, S.; Buyuktemiz, M.; Dede, Y.; Erten-Ela, S. *New J. Chem.* **2015**, *39*, 4086.
- (41) Watson, B. L.; Moore, T. A.; Moore, A. L.; Gust, D. *Dyes Pigm.* **2017**, *136*, 893.

- (42) Gayathri, T.; Barui, A. K.; Prashanthi, S.; Patra, C. R.; Singh, S. P. *RSC Adv.* **2014**, *4*, 47409.
- (43) Topel, S. D.; Topel, Ö.; Bostancıoğlu, R. B.; Koparal, A. T. *Colloids Surf., B* **2015**, *128*, 245.
- (44) Sui, B.; Tang, S.; Liu, T.; Kim, B.; Belfield, K. D. *ACS Appl. Mater. Interfaces* **2014**, *6*, 18408.
- (45) Fu, L.; Wang, F.-F.; Gao, T.; Huang, R.; He, H.; Jiang, F.-L.; Liu, Y. *Sens. Actuators, B* **2015**, *216*, 558.
- (46) Cao, X.; Lin, W.; Yu, Q.; Wang, J. *Org. Lett.* **2011**, *13*, 6098.
- (47) Zhu, S.; Zhang, J.; Janjanam, J.; Vegesna, G.; Luo, F.-T.; Tiwari, A.; Liu, H. *J. Mater. Chem. B* **2013**, *1*, 1722.
- (48) Zheng, K.; Chen, H.; Fang, S.; Wang, Y. *Sens. Actuators, B* **2016**, *233*, 193.
- (49) Greene, L. E.; Godin, R.; Cosa, G. *J. Am. Chem. Soc.* **2016**, *138*, 11327.
- (50) Kolehmainen, E.; Ośmiałowski, B.; Nissinen, M.; Kauppinen, R.; Gawinecki, R. *J. Chem. Soc. Perkin Trans. 2* **2000**, 2185.
- (51) Kolehmainen, E.; Ośmiałowski, B.; Krygowski, T. M.; Kauppinen, R.; Nissinen, M.; Gawinecki, R. *J. Chem. Soc. Perkin Trans. 2* **2000**, 1259.
- (52) Grabarz, A. M.; Laurent, A. D.; Jędrzejewska, B.; Zakrzewska, A.; Jacquemin, D.; Ośmiałowski, B. *J. Org. Chem.* **2016**, *81*, 2280.
- (53) Kucukoz, B.; Sevinc, G.; Yildiz, E.; Karatay, A.; Zhong, F.; Yilmaz, H.; Tutel, Y.; Hayvali, M.; Zhao, J.; Yaglioglu, H. G. *Phys. Chem. Chem. Phys.* **2016**, *18*, 13546.
- (54) Avlasevich, Y.; Li, C.; Mullen, K. *J. Mater. Chem.* **2010**, *20*, 3814.
- (55) Sun, Z.; Wu, J. *Aust. J. Chem.* **2011**, *64*, 519.
- (56) Hanson, K.; Roskop, L.; Djurovich, P. I.; Zahariev, F.; Gordon, M. S.; Thompson, M. E. *J. Am. Chem. Soc.* **2010**, *132*, 16247.
- (57) Kurotobi, K.; Kim, K. S.; Noh, S. B.; Kim, D.; Osuka, A. *Angew. Chem.* **2006**, *118*, 4048.
- (58) Kuisma, M. J.; Lundin, A. M.; Moth-Poulsen, K.; Hyldgaard, P.; Erhart, P. *J. Phys. Chem. C* **2016**, *120*, 3635.
- (59) Ośmiałowski, B.; Krygowski, T. M.; Dominikowska, J.; Palusiak, M. *New J. Chem.* **2011**, *35*, 1433.
- (60) Gawinecki, R.; Kolehmainen, E.; Loghmani-Khouzani, H.; Ośmiałowski, B.; Lovasz, T.; Rosa, P. *Eur. J. Org. Chem.* **2006**, *2006*, 2817.
- (61) Gresser, R.; Hummert, M.; Hartmann, H.; Leo, K.; Riede, M. *Chem. - Eur. J.* **2011**, *17*, 2939.
- (62) Yamazawa, S.; Nakashima, M.; Suda, Y.; Nishiyabu, R.; Kubo, Y. *J. Org. Chem.* **2016**, *81*, 1310.
- (63) Clar, E. *Aromatic Sextet*; Wiley: London, 1972.
- (64) Harvey, R. G. *Polycyclic Aromatic Hydrocarbons*; Wiley: New York, 1997.
- (65) Solà, M. *Frontiers in Chemistry* **2013**, *1*, 1.
- (66) Maksić, Z. B.; Barić, D.; Müller, T. *J. Phys. Chem. A* **2006**, *110*, 10135.
- (67) Krygowski, T. M.; Zachara, J. E.; Ośmiałowski, B.; Gawinecki, R. *J. Org. Chem.* **2006**, *71*, 7678.
- (68) Uppal, T.; Hu, X.; Fronczek, F. R.; Maschek, S.; Bobadova-Parvanova, P.; Vicente, M. G. H. *Chem. - Eur. J.* **2012**, *18*, 3893.
- (69) Kubo, Y.; Minowa, Y.; Shoda, T.; Takeshita, K. *Tetrahedron Lett.* **2010**, *51*, 1600.
- (70) Ni, Y.; Zeng, W.; Huang, K.-W.; Wu, J. *Chem. Commun.* **2013**, *49*, 1217.
- (71) Yang, L.; Liu, Y.; Ma, C.; Liu, W.; Li, Y.; Li, L. *Dyes Pigm.* **2015**, *122*, 1.
- (72) Jiao, L.; Yu, C.; Liu, M.; Wu, Y.; Cong, K.; Meng, T.; Wang, Y.; Hao, E. *J. Org. Chem.* **2010**, *75*, 6035.
- (73) Yu, C.; Xu, Y.; Jiao, L.; Zhou, J.; Wang, Z.; Hao, E. *Chem. - Eur. J.* **2012**, *18*, 6437.
- (74) Morgan, G. T.; Walls, L. P. *J. Chem. Soc.* **1931**, *0*, 2447.
- (75) Santoro, F.; Jacquemin, D. *WIREs Comput. Mol. Sci.* **2016**, *6*, 460.
- (76) Suppan, P. *J. Photochem. Photobiol., A* **1990**, *50*, 293.
- (77) Chaudhuri, T.; Shivran, N.; Mula, S.; Karmakar, A.; Chattopadhyay, S.; Chattopadhyay, S.; Bandyopadhyay, D. *RSC Adv.* **2016**, *6*, 59237.
- (78) Martin, A.; Long, C.; Forster, R. J.; Keyes, T. E. *Chem. Commun.* **2012**, *48*, 5617–5619.
- (79) Bröring, M.; Krüger, R.; Link, S.; Kleeberg, C.; Köhler, S.; Xie, X.; Ventura, B.; Flamigni, L. *Chem. - Eur. J.* **2008**, *14*, 2976–2983.
- (80) Chibani, S.; Laurent, A. D.; Le Guennic, B.; Jacquemin, D. *J. Chem. Theory Comput.* **2014**, *10*, 4574.
- (81) Le Guennic, B.; Jacquemin, D. *Acc. Chem. Res.* **2015**, *48*, 530.
- (82) Frisch, M. J.; Trucks, G. W.; Schlegel, H. B.; Scuseria, G. E.; Robb, M. A.; Cheeseman, J. R.; Scalmani, G.; Barone, V.; Mennucci, B.; Petersson, G. A.; Nakatsuji, H.; Caricato, M.; Li, X.; Hratchian, H. P.; Izmaylov, A. F.; Bloino, J.; Zheng, G.; Sonnenberg, J. L.; Hada, M.; Ehara, M.; Toyota, K.; Fukuda, R.; Hasegawa, J.; Ishida, M.; Nakajima, T.; Honda, Y.; Kitao, O.; Nakai, H.; Vreven, T.; Montgomery, J. A., Jr.; Peralta, J. E.; Ogliaro, F.; Bearpark, M.; Heyd, J. J.; Brothers, E.; Kudin, K. N.; Staroverov, V. N.; Kobayashi, R.; Normand, J.; Raghavachari, K.; Rendell, A.; Burant, J. C.; Iyengar, S. S.; Tomasi, J.; Cossi, M.; Rega, N.; Millam, J. M.; Klene, M.; Knox, J. E.; Cross, J. B.; Bakken, V.; Adamo, C.; Jaramillo, J.; Gomperts, R.; Stratmann, R. E.; Yazyev, O.; Austin, A. J.; Cammi, R.; Pomelli, C.; Ochterski, J. W.; Martin, R. L.; Morokuma, K.; Zakrzewski, V. G.; Voth, G. A.; Salvador, P.; Dannenberg, J. J.; Dapprich, S.; Daniels, A. D.; Farkas, Ö.; Foresman, J. B.; Ortiz, J. V.; Cioslowski, J.; Fox, D. J. *Gaussian 09*, Revision D.01; Gaussian, Inc.: Pittsburgh PA, 2009.
- (83) Shao, Y.; Gan, Z.; Epifanovsky, E.; Gilbert, A. T. B.; Wormit, M.; Kussmann, J.; Lange, A. W.; Behn, A.; Deng, J.; Feng, X.; Ghosh, D.; Goldey, M.; Horn, P. R.; Jacobson, L. D.; Kaliman, I.; Khaliullin, R. Z.; Kuš, T.; Landau, A.; Liu, J.; Proynov, E. I.; Rhee, Y. M.; Richard, R. M.; Rohrdanz, M. A.; Steele, R. P.; Sundstrom, E. J.; Woodcock, H. L.; Zimmerman, P. M.; Zuev, D.; Albrecht, B.; Alguire, E.; Austin, B.; Beran, G. J. O.; Bernard, Y. A.; Berquist, E.; Brandhorst, K.; Bravaya, K. B.; Brown, S. T.; Casanova, D.; Chang, C.-M.; Chen, Y.; Chien, S. H.; Closser, K. D.; Crittenden, D. L.; Diedenhofen, M.; DiStasio, R. A.; Do, H.; Dutoi, A. D.; Edgar, R. G.; Fatehi, S.; Fusti-Molnar, L.; Ghysels, A.; Golubeva-Zadorozhnaya, A.; Gomes, J.; Hanson-Heine, M. W. D.; Harbach, P. H. P.; Hauser, A. W.; Hohenstein, E. G.; Holden, Z. C.; Jagau, T.-C.; Ji, H.; Kaduk, B.; Khistyayev, K.; Kim, J.; Kim, J.; King, R. A.; Klunzinger, P.; Kosenkov, D.; Kowalczyk, T.; Krauter, C. M.; Lao, K. U.; Laurent, A. D.; Lawler, K. V.; Levchenko, S. V.; Lin, C. Y.; Liu, F.; Livshits, E.; Lochan, R. C.; Luenser, A.; Manohar, P.; Manzer, S. F.; Mao, S.-P.; Mardirossian, N.; Marenich, A. V.; Maurer, S. A.; Mayhall, N. J.; Neuscammann, E.; Oana, C. M.; Olivares-Amaya, R.; O'Neill, D. P.; Parkhill, J. A.; Perrine, T. M.; Peverati, R.; Prociuk, A.; Rehn, D. R.; Rosta, E.; Russ, N. J.; Sharada, S. M.; Sharma, S.; Small, D. W.; Sodt, A.; et al. *Mol. Phys.* **2015**, *113*, 184.
- (84) Tomasi, J.; Mennucci, B.; Cammi, R. *Chem. Rev.* **2005**, *105*, 2999.
- (85) Caricato, M.; Mennucci, B.; Tomasi, J.; Ingrosso, F.; Cammi, R.; Corni, S.; Scalmani, G. *J. Chem. Phys.* **2006**, *124*, 124520.
- (86) Zhao, Y.; Truhlar, D. *Theor. Chem. Acc.* **2008**, *120*, 215.
- (87) Petrenko, T.; Neese, F. *J. Chem. Phys.* **2007**, *127*, 164319.
- (88) Ferrer, F. J. A.; Improta, R.; Santoro, F.; Barone, V. *Phys. Chem. Chem. Phys.* **2011**, *13*, 17007.
- (89) Zaleśny, R.; Murugan, N. A.; Tian, G.; Medved', M.; Ågren, H. *J. Phys. Chem. B* **2016**, *120*, 2323.
- (90) Le Bahers, T.; Adamo, C.; Ciofini, I. *J. Chem. Theory Comput.* **2011**, *7*, 2498.
- (91) Jacquemin, D.; Bahers, T. L.; Adamo, C.; Ciofini, I. *Phys. Chem. Chem. Phys.* **2012**, *14*, 5383.